UCLA
UCLA Previously Published Works

Title

Ultra-high vacuum dc magnetron sputter-deposition of 0001-textured trigonal α-Ta2C/Al2O3(0001) thin films

Permalink

https://escholarship.org/uc/item/8410b9gf

Authors

Tanaka, Koichi
Aleman, Angel
Zaid, Hicham
et al.

Publication Date

2020-09-01

DOI

10.1016/j.mtla.2020.100838

Peer reviewed

eScholarship.org Powered by the California Digital Library
University of California

Author Manuscript

Author Manuscript

Author Manuscript

Author Manuscript

HHS Public Access

Author manuscript

Materialia (Oxf). Author manuscript; available in PMC 2022 November 17.

Published in final edited form as:

Materialia (Oxf). 2020 September ; 13: . doi:10.1016/j.mtla.2020.100838.

Ultra-high vacuum dc magnetron sputter-deposition of 0001-textured trigonal α-Ta_2C/Al_2O_3(0001) thin films

Koichi Tanaka[*,†], **Angel Aleman**[§], **Hicham Zaid**[†], **Michael E. Liao**[†], **Koki Hojo**[‡], **Yekan Wang**[†], **Mark S. Goorsky**[†], **Suneel Kodambaka**[†]

[†]Department of Materials Science and Engineering, University of California Los Angeles 410 Westwood Plaza, Los Angeles, CA 90095, USA

[§]Department of Mechanical and Aerospace Engineering, University of California Los Angeles, 420 Westwood Plaza, Los Angeles, CA 90095, USA

[‡]Graduate Department of Micro-Nano Mechanical Science and Engineering, Nagoya University, Furo-cho, Nagoya, Japan

Abstract

We report on the effects of substrate temperature (1073 K ≤ T_s ≤ 1373 K) and deposition time t (= 3 ~ 30 min.) on the crystallinity of Ta_2C/Al_2O_3(0001) thin films grown via ultra-high vacuum direct current magnetron sputtering of TaC target in 20 mTorr (2.7 Pa) pure Ar atmospheres. Using X-ray diffraction and transmission electron microscopy, we determine that the layers are 0001-oriented, trigonal-structured α-Ta_2C at all T_s. With increasing T_s, we obtain smoother and thinner layers with enhanced out-of-plane coherency and decreasing unit cell volume. Interestingly, the Ta_2C 0001 texture improves with increasing T_s up to 1273 K above which the layers are relatively more polycrystalline. At T_s = 1373 K, during early stages of deposition, the Ta_2C layers grow heteroepitaxially on Al_2O_3(0001) with $(0001)_{Ta_2C}\|(0001)_{Al_2O_3}$ and $[10\bar{1}0]_{Ta_2C}\|[11\bar{2}0]_{Al_2O_3}$. With increasing t, we observe the formation of anti-phase domains and misoriented grains resulting in polycrystalline layers. We attribute the observed enhancement in 0001 texture to increased surface adatom mobilities and the development of polycrystallinity to reduced incorporation of C in the lattice with increasing T_s. We expect that our results help develop methods for the synthesis of high-quality Ta_2C thin films.

Graphical Abstract

[*]Corresponding Author, koichitanaka@ucla.edu, Postal address: Engineering V 3111, 410 Westwood Plaza, Los Angeles, CA 90095, Tel: 310-848-7664.

Declaration of interests

The authors declare that they have no known competing financial interests or personal relationships that could have appeared to influence the work reported in this paper.

Publisher's Disclaimer: This is a PDF file of an unedited manuscript that has been accepted for publication. As a service to our customers we are providing this early version of the manuscript. The manuscript will undergo copyediting, typesetting, and review of the resulting proof before it is published in its final form. Please note that during the production process errors may be discovered which could affect the content, and all legal disclaimers that apply to the journal pertain.

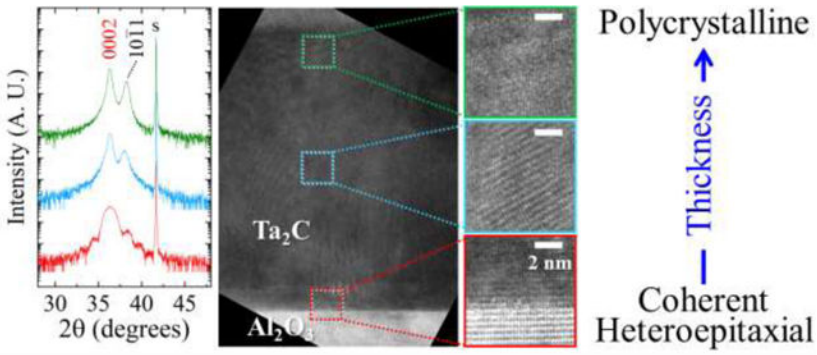

Keywords

Thin films; Tantalum; Carbides; UHTC; Epitaxial growth; Sputter deposition; Texture evolution

1. Introduction

Transition-metal carbides (TMCs) are ultra-high temperature ceramics used in a variety of applications as structural components in aerospace vehicles, cutting tools, as wear- and abrasion-resistant coatings, and as thin film gate electrodes in electronics owing to their exceptionally high melting points, high moduli, superior high-temperature mechanical properties, [1–4] and good electrical characteristics. [5–8] Among the TMCs, Ta-C compounds (Ta_2C, Ta_3C_2, Ta_4C_3, Ta_6C_5, and TaC) are known for their ultra-high melting points (for example, ~ 4250 K for rocksalt (B1) TaC and 3600 K for trigonal α-Ta_2C) [9] and their thermomechanical and electrical properties. [10–19] α-Ta_2C is relatively softer with superior ductility compared to B1-TaC at elevated temperatures [12] due to the operation of multiple slip systems. [12, 20, 21] B1-TaC is hard (25 GPa), [22] stiff (elastic modulus is 537 ~ 560 GPa), [23–25] and is known to exhibit localized plasticity [16, 26] at temperatures as low as 77 K and during compression of small-scale crystals at room-temperature. [27, 28] These studies suggest the possibility of improving the ductility and hence toughness of refractory carbides by engineering the composition, crystal size, and orientation. [28–30] One approach to controlling the microstructure is *via* bottom-up synthesis of thin films.

Ta-C thin films have been grown via evaporation, [31] pulsed laser deposition, [32] chemical vapor deposition, [33, 34] and more commonly via magnetron sputter-deposition. [2, 4–7, 35–38] While most of the existing literature is aimed at obtaining B1-TaC thin films, relatively few reported the growth of Ta_2C thin films; [5–8] other studies observed the unintentional formation of the Ta_2C phase. [36–38] Given the potential applications of Ta_2C in high-temperature structural applications, it is surprising that very little is known concerning the synthesis and microstructural evolution of Ta_2C. Here, we focus on understanding the growth-related aspects of sputter-deposited Ta_2C thin films.

In this paper, we report on the microstructural evolution in Ta_2C thin films deposited on single-crystalline Al_2O_3(0001) substrates via ultra-high vacuum (UHV) direct current (dc) magnetron sputtering of a TaC target in pure Ar discharges at substrate temperatures

Author Manuscript Author Manuscript Author Manuscript Author Manuscript

Author Manuscript Author Manuscript Author Manuscript Author Manuscript

T_s between 1073 K and 1373 K for times t up to 30 min. X-ray diffraction (XRD) and transmission electron microscopy (TEM) characterization of the as-deposited layers reveal the growth of α-Ta_2C thin films with 0001 preferred orientation at all T_s. We find that thickness decreases while both crystallinity and surface smoothness of the films improve monotonically with increasing T_s. We observe enhancement in 0001 texture with increasing T_s from 1073 K up to 1273 K. At higher T_s (= 1373 K), the thinner Ta_2C layers grow heteroepitaxially on Al_2O_3(0001) with the following crystallographic relationship $(0001)_{Ta_2C}\|(0001)_{Al_2O_3}$ and $[10\bar{1}0]_{Ta_2C}\|[11\bar{2}0]_{Al_2O_3}$ and develop polycrystallinity with increasing thickness. Based on these results, we suggest that the competition between enhanced surface mass transport and reduced carbon incorporation during deposition at elevated temperatures determine the morphology and texture of the Ta_2C thin films.

2. Experimental

All the Ta-C films are deposited on ~2 × 10 × 0.5 mm^3 Al_2O_3(0001) substrates in a dual-chamber UHV deposition system, details of which can be found in Refs. [36, 39–41]. Here, we present only the details specific to this report: base pressure p_B in the deposition chamber is 2×10^{-10} Torr (2.7×10^{-8} Pa). The substrates are cut out of 10 × 10 × 0.5 mm^3 Al_2O_3(0001) single-crystals (ACL101005S1 MTI Corp.), cleaned via ultrasonication for 10 minutes sequentially in acetone, isopropanol, and distilled water, blown dry using N_2 gas, and mounted on a sample holder. The sample holder is then transferred to the load-lock chamber, where it is held while the chamber is evacuated until the pressure is below 10^{-8} Torr (~ 10^{-6} Pa), after which the holder is transferred to the deposition chamber. The holder is fitted with a rectangular strip made of carbon nanotube yarn (5 × 15 × 0.15 mm^3, typical resistance: 2–3 Ω) that serves as a heating element and is used to thermally degas the sample-holder assembly. In our experiments, the samples are degassed at T_s = 1373 K in the UHV deposition chamber until p_B is below 6.0×10^{-9} Torr (8.0×10^{-7} Pa). *In situ* low-energy electron diffraction patterns (not shown) obtained from the samples prepared following this procedure reveal six-fold symmetric reflections, characteristic of clean, unreconstructed Al_2O_3(0001)-(1×1) surfaces. T_s is measured using an IMPAK IS 8-GS optical pyrometer and the measurement details are presented in Ref. [36]. Prior to deposition, T_s is set to desired value and Ta_2C films are deposited by dc magnetron sputtering of a 50.8 mm diameter × 3.18 mm thick TaC (99.5% purity, from Plasmaterials, Inc.) target in 20 mTorr (2.7 Pa) Ar (99.999%, Airgas Co.). The target power is held constant at 50 W and the layers are deposited for times t = 3, 5, 10, and 30 min. (The deposition rate R, as we show later, depends on the T_s and t and is between 0.04 and 0.05 nm/s.) The corresponding discharge current and voltage during sputter-deposition are 0.16 A and 297 ~ 302 V, respectively for all but the t = 3 min. sample deposited at T_s = 1373 K, for which we observe 0.18 A and 268 V. Following deposition, the samples are cooled passively to room temperature and characterized *ex situ* as described below.

XRD 2θ-ω measurements are carried out using a Bede D1 high-resolution diffractometer with monochromatic Cu $K_{\alpha 1}$ radiation wavelength λ is 0.154056 nm. XRD pole figures and ϕ scans are acquired using a Bede D1 rotary stage parallel beam diffractometer with non-monochromatic Cu X-rays following the procedures described in Ref. [36]. First, the

Author Manuscript Author Manuscript Author Manuscript Author Manuscript

samples are mounted on a miscut Si(100) wafer to eliminate background signal from the diffractometer stage. The optics of the detector and X-ray incident beam are calibrated to achieve maximum straight-through intensity. The sample inclinations are calibrated with respect to ω and χ (out-of-plane rotation perpendicular to ω) of Al_2O_3 0006 reflection at 2θ = 41.68° (JCPDS-ICDD No. 46–1212). 2θ-ω scans are obtained for 2θ values between 20° and 100° with a step size of 0.02° and a dwell time of 1 s. XRD pole figures of Al_2O_3 $11\bar{2}6$ and Ta_2C $10\bar{1}1$ reflections are acquired with 2θ fixed at 57.50° and 38.08°, respectively, and the desired reflection peak intensities measured along χ between 0° and 90° with a step size of 2.0°, and in-plane rotation angle ϕ between 0° and 360° with a step size of 1.0°. The dwell time is 1 s per step in these measurements. ϕ scans of Ta_2C $10\bar{1}2$ ($2\theta = 50.11°$) and Al_2O_3 $11\bar{2}6$ ($2\theta = 57.50°$) reflections are collected at $\chi = 42.6°$ and 42.3°, respectively, for ϕ from 0° to 360° with a step size of 0.05° and a dwell time of 0.5 s per step.

Cross-sectional transmission electron microscopy (XTEM) characterization is carried out on electron-transparent specimens prepared via focused ion beam (FIB) milling of the Ta-C thin films with 30 keV Ga^+ ions in an FEI Nova NanoLab™ 600 DualBeam FIB scanning electron microscope (FIB/SEM) system. Prior to milling, the film surface is protected by electron-beam-assisted deposition of ~100-nm-thick Pt layer from trimethyl platinum ($C_9H_{16}Pt$) using 30 kV and 0.1 nA electron beams. Although the Pt layer helps minimize Ga^+ implantation during milling, it results in unintentional deposition of carbon from the precursor. [42, 43] XTEM images of the films and the film/substrate interfaces are acquired using an FEI Titan scanning TEM (S/TEM) and a JEOL JEM-2800 TEM (S/TEM) operated at 300 kV and 200 kV, respectively.

3. Results and Discussion

Figure 1(a) shows typical 2θ-ω XRD scans obtained from Ta-C/Al_2O_3(0001) thin films sputter-deposited for t = 30 min. at T_s = 1073, 1173, 1223, 1273, and 1373 K. In the data, the peaks labeled **s** at 2θ = 41.68° and 90.76° are due to 0006 and 00012 reflections, respectively of the single-crystalline, corundum-structured Al_2O_3(0001) substrates (JCPDS-ICDD No. 46–1212) and the other peak at 2θ = 64.54° is a forbidden Al_2O_3 0009 reflection that is likely due to multiple reflections and/or substitutional impurities in the Al_2O_3(0001) crystals. [44, 45] To facilitate direct comparison of the XRD data across the samples, intensities in each of the curves are normalized to the highest intensities associated with Al_2O_3 00012 peak. The XRD data of the film deposited at the lowest T_s = 1073 K reveal broad overlapping peaks at 2θ values around 36°, 38°, 78°, and 82°. In comparison, the XRD data obtained from the films deposited at $T_s \geq 1173$ K show peaks at or close to 2θ = 36.32°, 38.24°, 59.46°, 77.16°, 82.02°, and 97.94°; we index these peaks as 0002, $10\bar{1}1$, $2\bar{1}\bar{1}0$, 0004, $20\bar{2}2$, and $3\bar{1}20$ reflections, respectively, of trigonal $\alpha - Ta_2C$ ($P\bar{3}\ m1$) [46] (For reference, Cu $K_{\alpha 1}$ XRD peaks of high-intensity reflections 111 and 002 of stoichiometric B1-TaC are expected at 2θ = 34.78° and 40.55°, respectively. [36]) The observation of multiple reflections is indicative of polycrystallinity. The XRD data of the samples grown at the higher T_s = 1273 and 1373 K show weaker intensity peaks labeled with asterisks at 2θ = 25.40° and 55.76°. While we are unable to attribute the peak at 25.40° to any of the possible Ta-C compounds or graphite (JCPDS-ICDD No. 41–1487),

Author Manuscript Author Manuscript Author Manuscript Author Manuscript

we suggest that the peak at 55.76° is likely due to α-Ta_2C 0003 reflection, expected at 2θ = 55.82°.

From the XRD data in Fig. 1(a), we measure full width at half maxima, Γ_{0002} and $\Gamma_{10\bar{1}1}$, respectively of 0002 and $10\bar{1}1$ peaks, the two primary reflections in α-Ta_2C, and their relative intensities $I_{0002}/I_{10\bar{1}1}$ at all T_s. Fig. 1(b) shows the T_s-dependent variations in $\Gamma_{0002}, \Gamma_{10\bar{1}1}$, and $I_{0002}/I_{10\bar{1}1}$. We find that the Γ values of both 0002 and $10\bar{1}1$ peaks decrease monotonically, indicative of increase in out-of-plane coherence length [47] and hence improved overall crystallinity, with increasing T_s. $I_{0002}/I_{10\bar{1}1}$ increases from 2.2 at T_s = 1073 K to 13.1 at T_s = 1273 K and decreases to 3.0 at T_s = 1373 K. Given that the strongest intensity reflection is $10\bar{1}1$ and $I_{0002}/I_{10\bar{1}1}$ is 0.253 in powder XRD of α-Ta_2C, [46] the fact that $I_{0002}/I_{10\bar{1}1} > 2$ for the films deposited at all $T_s \geq 1023$ K implies that the Ta_2C films are highly 0001-oriented at all T_s. In our experiments, the strongest 0001 texture is obtained in the films deposited at 1273 K. The observed decrease in $I_{0002}/I_{10\bar{1}1}$ upon further increase in T_s to 1373 K is suggestive of a disruption in 0001-oriented crystal growth, presumably due to change in the film composition.

We measure out-of-plane lattice parameters c from the peak positions of Ta_2C 0002 and 0004 reflections in Fig. 1(a) and use them as input to extract in-plane lattice parameters a from the 2θ values of $10\bar{1}1$, $20\bar{2}2$, and $3\bar{1}\bar{2}0$ reflections. Fig. 1(c) shows T_s-dependent variations in relative changes, $\varepsilon_a[= (a - a_o)/a_o]$, $\varepsilon_c[= (c - c_o)/c_o]$, and $\varepsilon_V[= (V - V_o)/V_o]$ in a, c, and unit cell volume $V\left(= 3\sqrt{3}a^2c/2\right)$ respectively, compared to the corresponding values $a_o(= 0.3103$ nm), $c_o(= 0.4938$ nm), and $V_o\left(= 0.1235\ \text{nm}^3\right)$ of bulk α-Ta_2C. [46] Errors associated with ε_a, ε_c, and ε_V are calculated from the measurement uncertainties associated with the a and c values extracted from the XRD data. We find that the a and c values of Ta_2C layers deposited at T_s = 1073 K are 1.5% larger and 0.6% smaller, respectively than the a_o and c_o values, yielding a 2.5% larger V compared to V_o. At $T_s \geq 1173$ K, the c values are, within the measurement uncertainties, the same as c_o and seemingly independent of T_s, whereas the a, and hence V, values decrease with increasing T_s. Given that the in-plane lattice mismatch is at least 13%, at 30° in-plane orientation, between α-Ta_2C(0001) and Al_2O_3(0001), significantly higher than the measured ε_a values, we suggest that the films are relaxed and attribute the observed T_s-dependent changes in a (and V) to variations in carbon content within the lattice. [36]

In order to better understand the effect of T_s on the development of microstructure within the Ta_2C layers, we carried out TEM characterization of the Ta_2C films. The top and bottom panels in Fig. 2 show typical (a-c) bright field and (d-f) high-angle annular dark field (HAADF) STEM images, respectively of the layers deposited at T_s = (a, d) 1073 K, (b, e) 1173 K, and (c, f) 1373 K. We find that the films deposited at lower T_s (= 1073 K) are relatively rough while those grown at higher T_s (= 1373 K) exhibit smoother surfaces. All the films, irrespective of the T_s, appear dense. From the XTEM images, we measure thicknesses of 91 ± 2.4 nm at 1073 K to 81 ± 1.6 nm at 1173 K, and 72.8 ± 0.9 nm at 1373 K, indicating that film thickness and hence R decrease with increasing T_s. Given

Author Manuscript Author Manuscript Author Manuscript Author Manuscript

that the substrate-film interfaces appear sharp irrespective of the T_s, we rule out interfacial reactions [39] and suggest that a reduction in sticking coefficient of the deposited species (most likely C) with increasing T_s as a possible reason for the observed decrease in film thickness. This is plausible since we observe the formation of C-deficient Ta_2C, rather than TaC, during sputter-deposition using nearly stoichiometric TaC target and consistent with previous results. [36] HAADF STEM images in Figs. 2(d) and (e) show fairly uniform contrast, suggestive of compositional homogeneity, across the films. However, Fig. 2(f) reveals distinctively darker contrast, characteristic of lighter atoms, with increasing thickness of the Ta_2C layer grown at higher T_s = 1373 K). Since the film is deposited *via* sputtering of TaC target in pure Ar atmosphere, we attribute the observed darker contrast in the upper portion of the film to increased carbon concentration, presumably due to surface segregation of C atoms during deposition.

In order to understand the spatial variations in composition and the suppression of 0001-texture at the highest T_s = 1373 K, we investigated the effect of thickness on the crystallinity of films grown at T_s = 1373 K. Fig. 3(a) shows 2θ-ω XRD scans obtained from the Ta_2C/Al_2O_3(0001) layers deposited for t = 3 and 10 min. along with the data from t = 30 min. sample shown in Fig. 1(a). We find primarily α-Ta_2C 0002 reflections for t = 3 min., 0002 and $10\bar{1}1$ reflections for t = 10 min., and multiple reflections for t = 30 min. The thinnest film (t = 3 min. sample) shows fringes (Laue oscillations) around 0002 peak, indicative of abrupt and/or high-quality substrate-film interfaces. With further increase in t, we observe a well-defined $10\bar{1}1$ reflection and $I_{0002}/I_{10\bar{1}1}$ decreases from 4.0 to 3.0 with increasing t from 10 to 30 min., indicative of reduced 0001-texture with increasing film thickness. Although 0001-texture is suppressed in thicker films, we find that Γ_{0002} decreases monotonically from 1.08° to 0.43° with increasing t from 3 to 30 min.; we attribute this result to an increase in out-of-plane coherent length with increasing thickness. From the peak positions of Ta_2C 0002 and 0004 reflections, we measure c values of 0.4938 ± 0.0001 nm, 0.4940 ± 0.0001, and 0.4941 ± 0.0001 nm for t = 3, 10, and 30 min. samples, respectively. The observed increase in c with t, although small, is suggestive of lattice distortion in the thicker films.

To identify the in-plane crystallographic relationship between Ta_2C(0001) and Al_2O_3(0001) at the onset of growth, we acquired XRD pole figures of Ta_2C $10\bar{1}1$ and Al_2O_3 $11\bar{2}6$ reflections from the Ta_2C/Al_2O_3(0001) film deposited for t = 3 min. at T_s = 1373 K and are presented as polar plots in Figs. 3(b) and 3(c), respectively. In obtaining the pole figures, since the Ta_2C film is highly 0001-oriented and the substrate is 0001-oriented Al_2O_3 single-crystal, we use 2θ values of 38.08° and 57.50°, respectively, corresponding to the bulk α – Ta_2C $10\bar{1}1$ and corundum-structured Al_2O_3 $11\bar{2}6$. We would like to point out that the 4-fold symmetric set of spots at χ = 20° in Fig. 3(c) are due to Si 222 reflections (2θ = 58.85°) from a miscut Si(100) wafer that is used to mount the samples. (In Fig. 3(b), we also find 3-fold symmetric spots at χ = 32°, origin of which is unknown.) In Figs. 3(b) and (c), we observe 6-fold symmetric Ta_2C $10\bar{1}1$ reflections at χ = 59 ± 1° and Al_2O_3 $11\bar{2}6$ reflections at χ = 39 ± 1°, respectively, at the same in-plane rotation angles φ = 0°, 60°, 120°, 180°, 240°, and 300°, indicating that Ta_2C $(10\bar{1}1)$ planes bear the same in-plane orientation as Al_2O_3 $(11\bar{2}6)$. We note that the measured angles χ = 59 ± 1° in

Author Manuscript Author Manuscript Author Manuscript Author Manuscript

Fig. 3(b) and 39 ± 1° in Fig. 3(c) are nearly the same as the calculated interplanar angles, 61.4° and 42.3°, respectively, between (0001) and $(10\bar{1}1)$ of α-Ta_2C and between (0001) and $(11\bar{2}6)$ of Al_2O_3. From these results, which are consistent with the φ scans (not shown), we conclude that the orientation relationships for ultra-thin Ta_2C film with respect to the $Al_2O_3(0001)$ substrate are: $(0001)_{Ta_2C}\|(0001)_{Al_2O_3}$ and $[10\bar{1}0]_{Ta_2C}\|[11\bar{2}0]_{Al_2O_3}$. These results show that the Ta_2C layers begin to grow heteroepitaxially on $Al_2O_3(0001)$ during early stages of sputter-deposition and become polycrystalline with increasing thickness.

In order to understand the transition from heteroepitaxial to polycrystalline growth, we carried out XTEM characterization of the thinner and thicker $Ta_2C/Al_2O_3(0001)$ films deposited at T_s = 1373 K and the data are presented in Figs. 4 and 5, respectively. Fig. 4(a) is a representative lattice-resolution XTEM image of the Ta_2C layer deposited for t = 5 min. From the image, we measure the thickness of the film as ~ 16 nm, i.e. R = 0.05 nm/s. (In comparison, Ta_2C layer grown for t = 30 min. at the same T_s using the same deposition parameters is ≈ 73 nm thick, see Figs. 2(c) and 5(a), corresponding to $R \approx$ 0.04 nm/s, suggestive of t-dependent R.) We find wavy features aligned nearly parallel to the substrate, which we attribute to stacking of basal planes in Ta_2C, consistent with the observation of high-intensity 0002 reflection in XRD data in Fig. 3(a). Figs. 4(b) and (c) are representative Fourier transforms (FT) obtained, respectively from the regions bounded by yellow (Ta_2C film) and red (Al_2O_3 substrate) dotted squares in Fig. 4(a). We do not observe $10\bar{1}1$ spots in Fig. 4(b). From the observed symmetry of the reflections in Figs. 4(b) and (c), we identify the orientation relationship between the Ta_2C film and the substrate as $(0001)_{Ta_2C}\|(0001)_{Al_2O_3}$ and $[10\bar{1}0]_{Ta_2C}\|[11\bar{2}0]_{Al_2O_3}$. These results indicate that the film is highly 0001-oriented and exhibits the same orientation relationship with the substrate as the thinner (t = 3 min.) sample. Fig. 4(d) is a higher magnification TEM image of a portion of Fig. 4(a), highlighted by a green dotted square, showing layer stacking and a defect indicated by an arrow. In α-Ta_2C, along 0001, individual layers of C and Ta atoms are stacked on top of each other as αBCαBCα…, analogous to ABCABCA... stacking in 111-oriented face-centered cubic lattice, with capital and Greek letters corresponding to Ta and C layers, respectively. [10, 48] Defects in stacking may occur as a result of C-vacancies and result in the formation of anti-phase domains, i.e. domains with AβCAβCA… or ABγABγA… stacking instead of the ideal αBCαBCα…stacking. However, additional high-resolution TEM characterization is required to accurately determine the structure of these features.

Fig. 5(a) is a representative bright-field XTEM image of the thicker Ta_2C film deposited for t = 30 min. We find contrast undulations that appear as parallel ‘stripes’, most of which are oriented along the growth direction. A high-resolution TEM image of the region bounded by a cyan dotted square in Fig. 5(a) is shown in Fig. 5(b). The image shows a portion of the substrate-film interface, where we observe atomic columns in the film aligned with those in the substrate, suggestive of coherent growth of Ta_2C film on $Al_2O_3(0001)$ substrate. Inset in Fig. 5(b) is a FT of the entire field of view, in which we find only one set of reflections, consistent with our conclusion above. Figs. 5(c)-(f) are FTs of four regions from near the substrate-film interface up to the top of the film. Near the interface [Fig. 5(c)], the Ta_2C film exhibits 0001 orientation along the growth direction. At film thicknesses ~10 nm and farther

Author Manuscript Author Manuscript Author Manuscript Author Manuscript

from the interface [Figs. 5(d) and (e)], we observe 17° ~ 29° tilt in the 0001-oriented grains. Eventually, near the top of the film [Fig. 5(f)], we find grains with $1\bar{1}02$ orientation. These results, which show the transition from fully coherent 0001-oriented growth to a different orientation with increasing thickness, are consistent with the XRD results in Fig. 3(a).

To consistently explain the observed T_s and t dependent evolution of crystallinity in sputter-deposited Ta_2C thin films, we propose the following: crystallinity of the Ta-C layers deposited via sputtering of TaC target in inert Ar gas discharges depends on the carbon content in the lattice. Under our experimental conditions, we know that not all C released during sputtering of the TaC target is incorporated into the films deposited on oxide substrates at high T_s, a result of which is the growth of Ta_2C instead of TaC. [36] Since the adatom mobilities on refractory transition-metal compound surfaces are generally associated with high activation barriers, [49, 50] we expect that increasing T_s leads to enhanced surface mass transport and favors the formation of lower-energy {0001} surfaces, resulting in 0001-oriented films with smoother surfaces (see Figs. 1 and 2). An unintended consequence of increasing T_s, however, is the disproportionate reduction in the sticking coefficient of the incident C atoms compared to that of Ta atoms; here, we assume that the sticking coefficient of the lighter element C decreases more than that of the heavier Ta at the T_s (1073 ~ 1373 K) used in our experiments. As a result, the C content in the film decreases with increasing both T_s and t, consistent with the observed decrease in R with T_s (Fig. 2) and t (compare the thicknesses of layers in Figs. 4 and 5). The change in C-content leads to lattice distortion [see for example Fig. 1(c)] during early stages of deposition followed by the formation of anti-phase domains [e.g., Fig. 4(d)] and eventually result in the growth of grains with other orientations as observed in Figs. 3 and 5.

4. Conclusions

In summary, we investigated the effects of substrate temperature (1073 K ≤ T_s ≤ 1373 K) and deposition time on microstructural evolution of $Ta_2C/Al_2O_3(0001)$ thin films grown *via* UHV dc magnetron sputtering of TaC target in pure Ar atmospheres. We obtain 0001-oriented, trigonal-structured α-Ta_2C films that are increasingly smoother and thinner with increasing T_s. The 0001-texture improves with increasing T_s up to 1273 K. At T_s = 1373 K, we observe highly coherent 0001-oriented growth with the following orientation relationship: $(0001)_{Ta_2C}\|(0001)_{Al_2O_3}$ and $[10\bar{1}0]_{Ta_2C}\|[11\bar{2}0]_{Al_2O_3}$ during the early stages of deposition followed by the formation of anti-phase domains and misoriented grains at the later times yielding polycrystalline layers with reduced 0001-texture. We attribute the improvement in film smoothness, crystallinity, and the 0001-texture with increasing T_s to increased surface adatom mobilities and the decrease in film thickness and the disruption in heteroepitaxial growth to the reduced incorporation of C leading to the formation of structural defects. We expect that our results provide new insights into the factors influencing the crystallinity of sputter-deposited α-Ta_2C thin films.

ACKNOWLEDGEMENTS

We gratefully acknowledge support from the Air Force Office of Scientific Research (AFOSR, Dr. Ali Sayir) under Grant # FA9550-14-1-0106 and # FA9550-18-1-0050. KT is supported by the Japan Student Service Organization (L16111111026) and the UCLA graduate division fellowships for his doctoral study in the United States. AA is

Author Manuscript Author Manuscript Author Manuscript Author Manuscript

supported by the National Science Foundation (NSF CMMI) grant #1563427 (Dr. Kara Peters). KH is supported by the Japan-US Advanced Collaborative Education Program (JUACEP). We thank Mr. Noah Bodzin and the Nanoelectronics Research Facility in the UCLA Henry Samueli School of Engineering for assistance with focused ion beam milling. We acknowledge the use of instruments at the Electron Imaging Center for NanoMachines supported by NIH (1S10RR23057) and the California NanoSystems Institute at UCLA and transmission electron microscopy at the Irvine Materials Research Institute (IMRI), part of the University of California Irvine.

References

[1]. Williams WS, Transition-Metal Carbides, Prog. Solid State Chem 6 (1971) 57–118.

[2]. Håkansson G, Petrov I, Sundgren JE, Growth of TaC thin films by reactive direct current magnetron sputtering: Composition and structure, J. Vac. Sci. Technol. A 8(5) (1990) 3769–3778.

[3]. Hugosson HW, Jansson U, Johansson B, Eriksson O, Restricting dislocation movement in transition metal carbides by phase stability tuning, Science 293 (2001) 2434–2437. [PubMed: 11577231]

[4]. Tuleushev YZ, Volodin VN, Zhakanbaev EA, Alimzhan B, Structure and phase composition of deposited tantalum–carbon films, The Physics of Metals and Metallography 117(8) (2016) 789–794.

[5]. Chang SZ, Yu HY, Adelmann C, Delabie A, Wang XP, Van Elshocht S, Akheyar A, Nyns L, Swerts J, Aoulaiche M, Kerner C, Absil P, Hoffmann TY, Biesemans S, Electrical Properties of Low-VT Metal-Gated n-MOSFETs Using La2O3/SiOx as Interfacial Layer Between HfLaO High-κ Dielectrics and Si Channel, IEEE Electron Device Letters 29(5) (2008) 430–433.

[6]. Simoen E, Akheyar A, Rohr E, Merch A, Claeys C, Low-frequency Noise Analysis of the Impact of an LaO Cap Layer in HfSiON/Ta2C Gate Stack nMOSFETs, ECS Trans. 25 (2009) 237–245.

[7]. Crupi F, Magnone P, Simoen E, Pantisano L, Giusi G, Pace C, Claeys C, The Role of the Interfaces in the 1/f Noise of MOSFETs with High-k Gate Stacks, ECS Trans. 19(2) (2009) 87–99.

[8]. O'Sullivan BJ, Pourtois G, Kaushik VS, Schram T, Kittl JA, Pantisano L, De Gendt S, Heyns M, Charge characterization in metal-gate/high-κ layers: Effect of post-deposition annealing and gate electrode, Appl. Phys. Lett 91(3) (2007).

[9]. Gusev AI, Kurlov AS, Lipatnikov VN, Atomic and vacancy ordering in carbide ζ-Ta4C3−x (0.28≤x≤0.40) and phase equilibria in the Ta–C system, J. Solid State Chem 180(11) (2007) 3234–3246.

[10]. Yu X-X, Weinberger CR, Thompson GB, *Ab initio* investigations of the phase stability in tantalum carbides, Acta Mater. 80 (2014) 341–349.

[11]. Giorgi AL, Szklarz EG, Storms EK, Bowman AL, Investigation ofTa2C,Nb2C, andV2C for Superconductivity, Phys. Rev 129(4) (1963) 1524–1525.

[12]. De Leon N, Wang B, Weinberger CR, Matson LE, Thompson GB, Elevated-temperature deformation mechanisms in Ta_2C: An experimental study, Acta Mater. 61(11) (2013) 3905–3913.

[13]. Desmaison-Brut M, Alexandre N, Desmaison J, Comparison of the Oxidation Behaviour of Two Dense Hot Isostatically Pressed Tantalum Carbide (TaC and Ta2C) Materials, J. Euro. Ceram. Soc 17 (1997) 1325–1334.

[14]. Khyzhun OY, XPS XES, and XAS studies of the electronic structure of substoichiometric cubic TaCx and hexagonal Ta2Cy carbides, Journal of Alloys and Compounds 259(1–2) (1997) 47–58.

[15]. Alexandre N, Desmaison-Brut M, Valin F, Boncoeur M, Solid State Reaction between Tantalum (Ta) and Tantalum Carbide (TaC) Powders during Hiping, Key Engineering Materials 132–136 (1997) 868–871.

[16]. Rowcliffe DJ, Hollox GE, Plastic Flow and Fracture of Tantalum Carbide and Hafnium Carbide at Low Temperatures, J. Mat. Sci 6 (1971) 1261–1269.

[17]. De Leon N, Yu XX, Yu H, Weinberger CR, Thompson GB, Bonding effects on the slip differences in the B1 monocarbides, Phys. Rev. Lett 114(16) (2015) 165502.

[18]. Gusev AI, Sequence of phase transformations in the formation of superstructures of the M6C5 type in nonstoichiometric carbides, Journal of Experimental and Theoretical Physics 109(3) (2009) 417–433.

[19]. Lipatnikov VN, Gusev AI, Atomic-vacancy ordering in the carbide phase ζ-Ta4C3-x, Physics of the Solid State 48(9) (2006) 1634–1645.

Author Manuscript Author Manuscript Author Manuscript Author Manuscript

[20]. De Leon N, Wang B, Weinberger C, Thompson G, Elevated Temperature Deformation Mechanisms in Ta2C, Microscopy and Microanalysis 17(S2) (2011) 1898–1899.

[21]. Wang B, De Leon N, Weinberger CR, Thompson GB, A theoretical investigation of the slip systems of Ta2C, Acta Mater. 61(11) (2013) 3914–3922.

[22]. Toth LE, Transition Metal Carbides and Nitrides, Academic Press, New York City, New York, 1971.

[23]. Holleck H, Material selection for hard coatings, J. Vac. Sci. Technol. A 4(6) (1986) 2661–2669.

[24]. López-de-la-Torre L, Winkler B, Schreuer J, Knorr K, Avalos-Borja M, Elastic properties of tantalum carbide (TaC), Solid State Communications 134(4) (2005) 245–250.

[25]. Brown HL, Armstrong PE, Kempter CP, Elastic Properties of Some Polycrystalline Transition-Metal Monocarbides, J. Chem. Phys 45(2) (1966) 547–549.

[26]. Gusev AI, Rempel AA, Magerl AJ, Disorder and Order in Strongly Nonstoichiometric Compounds: Transition Metal Carbides, Nitrides and Oxides, 2nd ed., Springer Science and Business Media, Berlin - Heidelberg, 2013.

[27]. Kiani S, Ratsch C, Minor AM, Yang JM, Kodambaka S, In situ transmission electron microscopy observations of room-temperature plasticity in sub-micron-size TaC(100) and TaC(011) single crystals, Scripta Materialia 100 (2015) 13–16.

[28]. Kiani S, Yang J-M, Kodambaka S, Nanomechanics of Refractory Transition-Metal Carbides: A Path to Discovering Plasticity in Hard Ceramics, J. Am. Ceram. Soc 98(8) (2015) 2313–2323.

[29]. Kiani S, Leung KWK, Radmilovic V, Minor AM, Yang JM, Warner DH, Kodambaka S, Dislocation glide-controlled room-temperature plasticity in 6H-SiC single crystals, Acta Mater. 80(0) (2014) 400–406.

[30]. Kiani S, Ratsch C, Minor AM, Kodambaka S, Yang JM, Orientation- and size-dependent room-temperature plasticity in ZrC crystals, Philosophical Magazine 95(9) (2015) 985–997.

[31]. Naiki T, Ninomiya M, Ihara M, Epitaxial Growth of Tantalum Carbide, Japan. J. Appl. Phys 11 (1972) 1106.

[32]. Teghil R, D'Alessio L, Zaccagnino M, Ferro D, Marotta V, Maria GD, TiC and TaC deposition by pulsed laser ablation: a comparative approach, Appl. Surf. Sci 173 (2001) 233–241.

[33]. Kim D, Jeong SM, Yoon SG, Woo CH, Kim JI, Lee H-G, Park JY, Kim W-J, Chemical Vapor Deposition of Tantalum Carbide from TaCl5-C3H6-Ar-H2 System, Journal of the Korean Ceramic Society 53(6) (2016) 597–603.

[34]. Ali M, Ürgen M, Atta MA, Tantalum carbide films synthesized by hot-filament chemical vapor deposition technique, Surf. Coat. Technol 206(11–12) (2012) 2833–2838.

[35]. Vargas M, Castillo HA, Restrepo-Parra E, De La Cruz W, Stoichiometry behavior of TaN, TaCN and TaC thin films produced by magnetron sputtering, Appl. Surf. Sci 279 (2013) 7–12.

[36]. Tanaka K, Aleman A, Liao ME, Wang Y, Goorsky MS, Kodambaka S, Effects of ultra-low ethylene partial pressure on microstructure and composition of reactively sputter-deposited Ta–C thin films, Thin Solid Films 688 (2019) 137440.

[37]. Lasfargues H, Glechner T, Koller CM, Paneta V, Primetzhofer D, Kolozsvári S, Holec D, Riedl H, Mayrhofer PH, Non-reactively sputtered ultra-high temperature Hf-C and Ta-C coatings, Surf. Coat. Technol 309 (2017) 436–444.

[38]. Riedl H, Glechner T, Wojcik T, Koutná N, Kolozsvári S, Paneta V, Holec D, Primetzhofer D, Mayrhofer PH, Influence of carbon deficiency on phase formation and thermal stability of super-hard TaC_y thin films, Scripta Materialia 149 (2018) 150–154.

[39]. Tanaka K, Fankhauser J, Zaid H, Aleman A, Sato M, Yu D, Ebnonnasir A, Li C, Kobashi M, Goorsky MS, Kodambaka S, Kinetics of Zr-Al intermetallic compound formation during ultra-high vacuum magnetron sputter-deposition of Zr/Al2O3(0001) thin films, Acta Mater. 152 (2018) 34–40.

[40]. Aleman A, Li C, Zaid H, Kindlund H, Fankhauser J, Prikhodko SV, Goorsky MS, Kodambaka S, Ultrahigh vacuum dc magnetron sputter-deposition of epitaxial Pd(111)/Al2O3(0001) thin films, J. Vac. Sci. Technol. A 36(3) (2018) 030602.

[41]. Fankhauser J, Sato M, Yu D, Ebnonnasir A, Kobashi M, Goorsky MS, Kodambaka S, Growth and characterization of epitaxial Zr(0001) thin films on Al2O3(0001), J. Vac. Sci. Technol. A 34(5) (2016) 050606.

Author Manuscript Author Manuscript Author Manuscript Author Manuscript

[42]. Kodambaka S, Ngo C, Palisaitis J, Mayrhofer PH, Hultman L, Persson POÅ, Kinetics of Ga droplet decay on thin carbon films, Appl. Phys. Lett 102(16) (2013) 161601.

[43]. Jouanny I, Palisaitis J, Ngo C, Mayrhofer PH, Hultman L, Persson POÅ, Kodambaka S, In situ transmission electron microscopy studies of the kinetics of Pt-Mo alloy diffusion in ZrB_2 thin films, Appl. Phys. Lett 103(12) (2013) 121601.

[44]. Inaba K, Kobayashi S, Uehara K, Okada A, Reddy SL, Endo T, High Resolution X-Ray Diffraction Analyses of (La,Sr)MnO3/ZnO/Sapphire(0001) Double Heteroepitaxial Films, Adv. Mater. Phys. Chem 03(01) (2013) 72–89.

[45]. Anderson AA, Eason RW, Jelinek M, Grivas C, Lane D, Rogers K, Hickey LMB, Fotakis C, Growth of Ti:sapphire single crystal thin films by pulsed laser deposition, Thin Solid Films 300 (1997) 68–71.

[46]. Bowman AL, Wallace TC, Yarnell JL, Wenzel RG, Storms EK, The Crystal Structures of V2C and Ta2C, Acta Crystallographica 19 (1965) 6.

[47]. Lee T, Seo H, Hwang H, Howe B, Kodambaka S, Greene JE, Petrov I, Fully strained low-temperature epitaxy of TiN/MgO(001) layers using high-flux, low-energy ion irradiation during reactive magnetron sputter deposition, Thin Solid Films 518(18) (2010) 5169–5172.

[48]. Yu H, Guziewski M, Thompson GB, Weinberger CR, A model for understanding the formation energies of nanolamellar phases in transition metal carbides and nitrides, Modelling and Simulation in Materials Science and Engineering 24(5) (2016) 055004.

[49]. Kodambaka S, Petrova V, Vailionis A, Desjardins P, Cahill DG, Petrov I, Greene JE, In-situ high-temperature scanning-tunnelling-microscopy studies of two-dimensional island-decay kinetics on atomically smooth TiN(001), Surface Review and Letters 7(5–6) (2000) 589–593.

[50]. Kodambaka S, Israeli N, Bareno J, Swiech W, Ohmori K, Petrov I, Greene JE, Low-energy electron microscopy studies of interlayer mass transport kinetics on TiN(111), Surface Science 560(1–3) (2004) 53–62.

Author Manuscript Author Manuscript Author Manuscript Author Manuscript

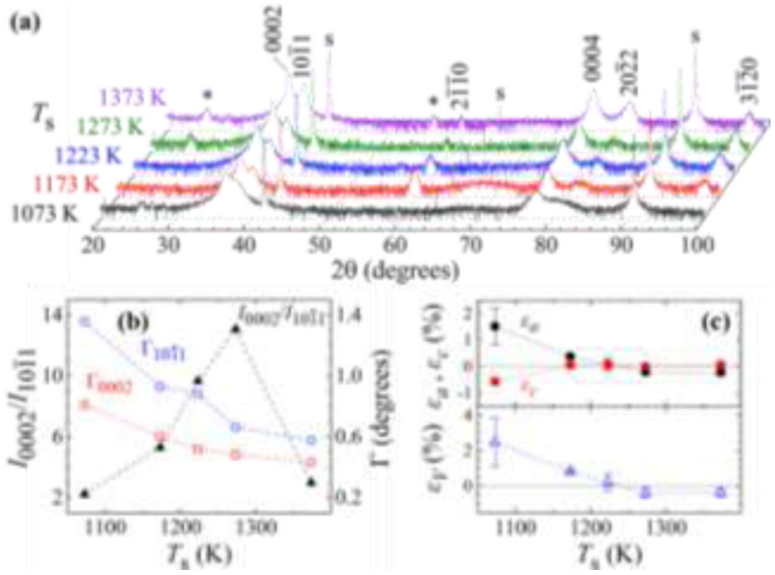

Figure 1.

(a) Representative 2θ-ω X-ray diffraction (XRD) scans, color coded for clarity, obtained from $Ta_2C/Al_2O_3(0001)$ thin films sputter-deposited for times t = 30 min. at different T_s. Intensities in each of the curves are normalized to the intensity of the Al_2O_3 00012 reflection and are plotted on a logarithmic scale. Labels **s** indicate the peaks due to Al_2O_3 000l reflections with l = 6, 9, and 12 at progressively increasing 2θ values. Unidentified peaks are assigned asterisks and are discussed in the text. (b) Plots of full width at half maxima, $\Gamma_{10\bar{1}1}$ (open circles) and Γ_{0002} (open squares) of $10\bar{1}1$ and 0002 reflection peaks respectively, and their relative intensity ratios [$I_{0002}/I_{10\bar{1}1}$ (filled triangles)] as a function of T_s. (c) Plots of ε_a (solid circles), ε_c (solid squares), and ε_V (open triangles) vs. T_s, where a (c) is the in-plane (out-of-plane) lattice parameter of α-Ta_2C, extracted from the XRD scans in (a), $V\left[=(3\sqrt{3}/2)a^2c\right]$ is the unit cell volume, and $\varepsilon_i = [(i - i_0)/i_0] \times 100$, with i = a, c, and V. a_o(= 0.3103 nm), c_o(= 0.4938 nm), and $V_o\left(=0.1235\ \text{nm}^3\right)$ correspond to bulk $\alpha - Ta_2C$ ($P\bar{3}m1$). [46]

Author Manuscript Author Manuscript Author Manuscript Author Manuscript

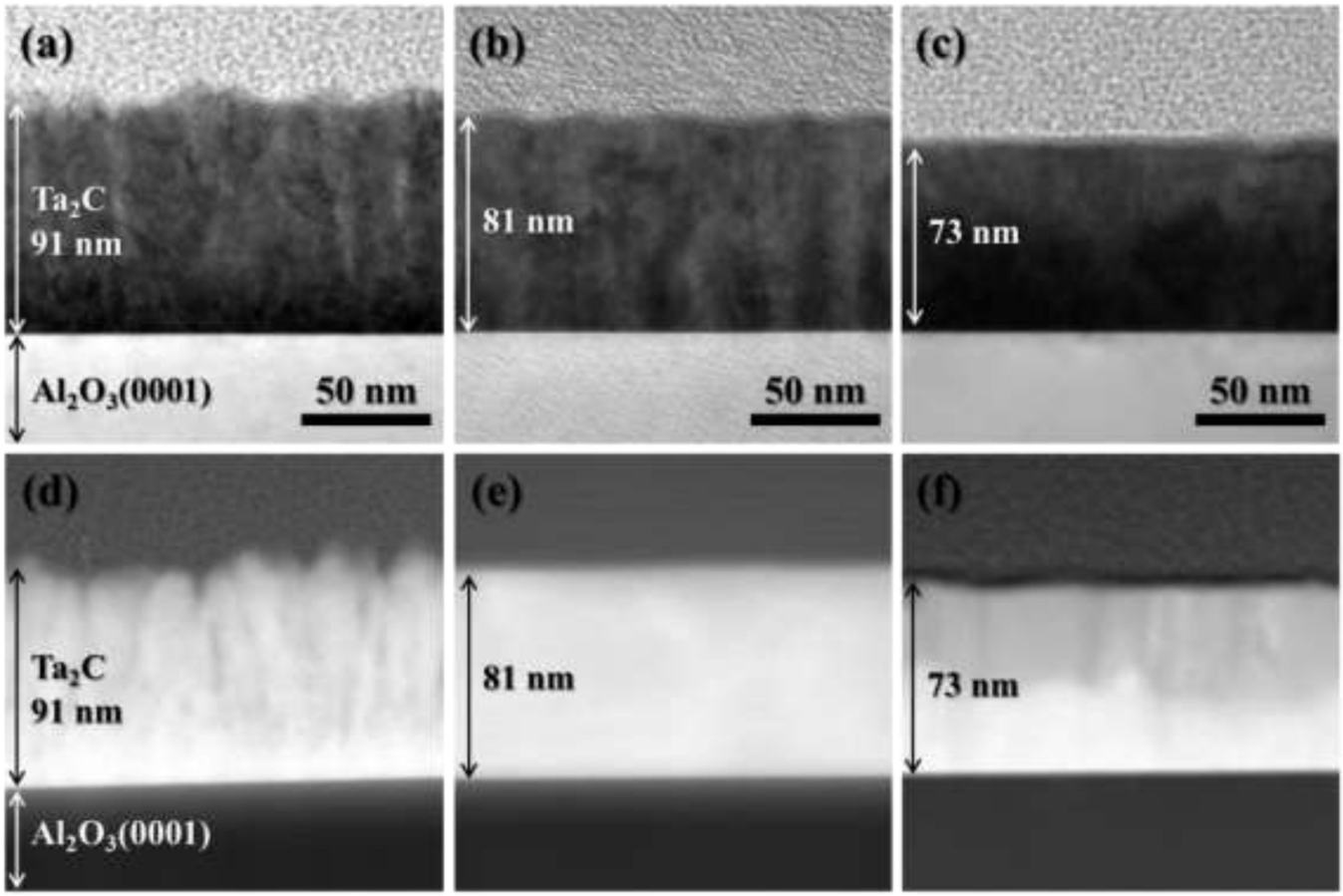

Figure 2.

(top) Cross-sectional transmission electron microscopy (XTEM) and (bottom) high-angle annular dark field scanning TEM images obtained from $Ta_2C/Al_2O_3(0001)$ films sputter-deposited for t = 30 min. at T_s = (a,d) 1073 K, (b,e) 1173 K, and (c,f) 1373 K.

Author Manuscript Author Manuscript Author Manuscript Author Manuscript

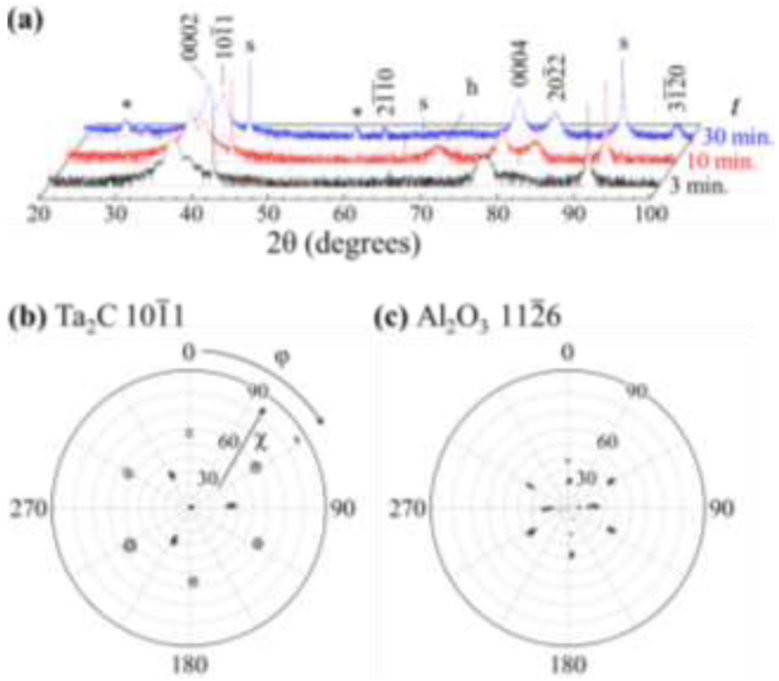

Figure 3.

(a) Plot of 2θ-ω XRD data obtained from $Ta_2C/Al_2O_3(0001)$ layers sputter-deposited at T_s = 1373 K for t = 3, 10, and 30 min. with intensities in each of the curves normalized to those of the Al_2O_3 00012 reflections and plotted on logarithmic scale. (Please note that the time axis is not to scale.) Peaks due to α-Ta_2C reflections are labeled as shown. **s** refers to Al_2O_3 000l reflections with l = 6, 9, and 12 at progressively increasing 2θ values. **h** indicates background scattering from the sample holder. Please see the text for discussion on the peaks assigned asterisks. (b, c) XRD pole figures of (b) Ta_2C 10$\bar{1}$1 and (c) Al_2O_3 11$\bar{2}$6 reflections obtained from the sample deposited at 1373 K for t = 3 min.

Author Manuscript Author Manuscript Author Manuscript Author Manuscript

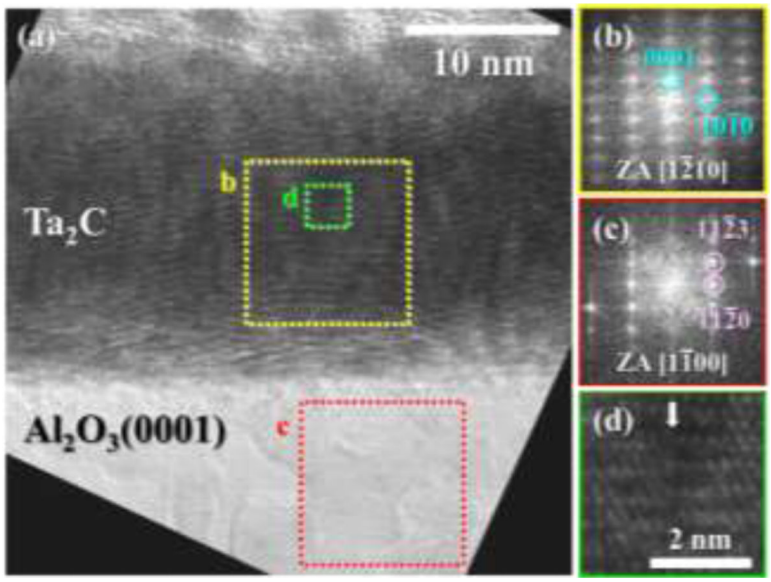

Figure 4.

(a) Representative XTEM image of the $Ta_2C/Al_2O_3(0001)$ film deposited at T_s = 1373 K for t = 5 min. (b and c) Fourier transforms (FTs) of (b) yellow (Ta_2C) and (c) red (Al_2O_3) dotted square regions, respectively in (a). In (b) and (c), two of the film and substrate reflections are highlighted, respectively using cyan and purple circles, and ZA refers to zone axis. (d) Higher magnification TEM image of the green dotted square labeled **d** in (b). Arrow in (d) shows incoherency in layer stacking.

Author Manuscript Author Manuscript Author Manuscript Author Manuscript

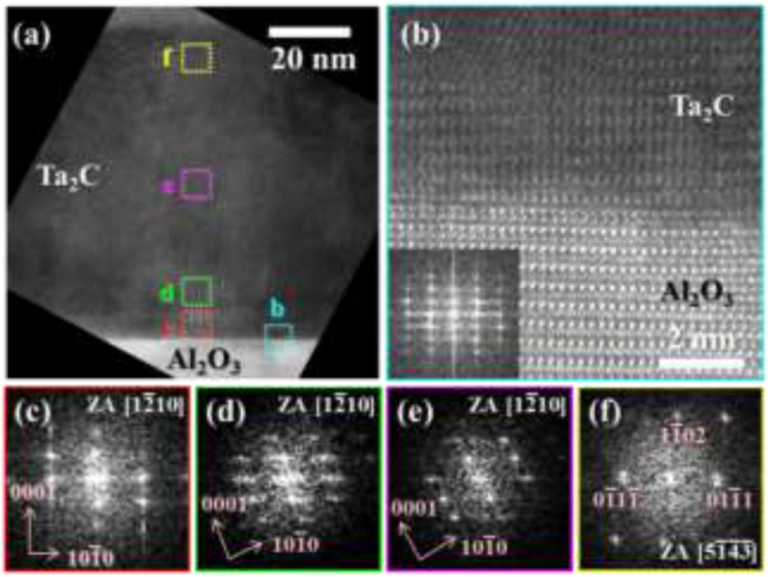

Figure 5.

(a) Typical XTEM image of the $Ta_2C/Al_2O_3(0001)$ film deposited at T_s = 1373 K for t = 30 min. (b) Higher resolution TEM image with inset showing FT of the region bounded by a cyan dotted square labeled **b** in (a). (c - f) FTs of the (c) red, (d) green, (e) pink, and (f) yellow dotted square areas in (a). In the FTs, ZA refers to zone axis.